All Non-vacuum Processed CIGS Solar Cells Using Scalable Ag NWs/AZO based Transparent Electrode

Journal:	*ACS Applied Materials & Interfaces*
Manuscript ID	am-2016-021372.R2
Manuscript Type:	Article
Date Submitted by the Author:	02-Jun-2016
Complete List of Authors:	Wang, Mingqing; University College London, UCL Institute for Materials Discovery Choy, Kwang-Leong; University College London, UCL Institute for Materials Discovery

SCHOLARONE™
Manuscripts

All Non-vacuum Processed CIGS Solar Cells Using Scalable Ag NWs/AZO based Transparent Electrode

Mingqing Wang, Kwang-Leong Choy*.

UCL Institute for Materials Discovery, University College London, Roberts Building, Malet Place, London, WC1E 7JE, United Kingdom.

KEYWORDS: CIGS solar cells; Ag nanowires; non-vacuum; transparent conducting electrode; nanocomposite

Abstract: With record cell efficiency of 21.7%, CIGS solar cells have demonstrated to be a very promising photovoltaic (PV) technology. However, their market penetration has been limited due to the inherent high cost of the cells. In this work, in order to lower the cost of CIGS solar cells, all non-vacuum processed CIGS solar cells were designed and developed. CIGS absorber was prepared by annealing of electrodeposited metallic layers in chalcogen atmosphere. Non-vacuum deposited Ag nanowires(NWs)/AZO transparent electrodes(TEs) with good transmittance (92.0% at 550nm) and high conductivity(sheet resistance of 20 $\Omega/\square$) were used to replace the vacuum sputtered window layer. Additional thermal treatment after device preparation was conducted at 220℃ for a few of minutes to improve both the value and the uniformity of the efficiency of CIGS pixel cell on 5cm x 5cm substrate. The best performance of the all non-

vacuum fabricated CIGS solar cells showed efficiency of 14.05% with Jsc of 34.82mA/cm^2, Voc of 0.58V and FF of 69.60% respectively, which is comparable with the efficiency of 14.45% of a reference cell using sputtered window layer.

Introduction

Chalcopyrite CuInGaSe$_2$ (CIGS) thin film based solar cells have the highest efficiency in all of the thin film PV technology, recently achieving above 21.7% at cell level[1]. In addition to the high efficiency, CIGS solar cells also exhibit other advantages such as a higher performance ratio and lower energy payback time compared to Silicon, very good stability as compared with organic solar cells or organic/inorganic hybrid solar cells, establishing it as one of the most promising commercial thin film solar modules. However, market penetration of CIGS cells has been limited due to the inherent high cost and low deposition rate of the existing physical vapour deposition (PVD) based vacuum techniques employed in their manufacturing. In order to make the CIGS solar industry competitive and sustainable in the long-term, CIGS absorbers using low cost and non-vacuum processes (e.g. electrodeposition[2], hydrazine[3], quaternary nanoparticles[4], and other wet chemical route using precursor such as metal salts[5], metal sulphides[6], and metal oxide[7]) have been developed. Electrodeposition (ED) is a maturely developed technology for production of commercial metallic film coatings[8]. As compared with other non-vacuum techniques, ED shows the advantages of high deposition rate and high material utilization. Large scale industrial research on electrodeposition based CIGS cells has reached solar cells with pixel efficiency of 15.3% by Solopower[9]and 17.3% by Nexcis[10].

The cost of CIGS solar cells can be further reduced through investigating the application of non-vacuum deposited window layer to replace sputter deposited intrinsic-ZnO(i-ZnO)/

transparent conducting oxide (TCO) bilayer. Yaroslav et al published their work on all solution

processed chalogenide solar cells using CBD (Chemical Bath Deposition) grown aluminum

doped ZnO (AZO) as front contact[11]. As compared with other chemical process, the CBD

method tends to suffer more from the reproducibility and wastage of solution after every

deposition, which has environmental impact and concern. Tsin et al applied electrodeposited

transparent conductive chlorine doped ZnO layer together with sputtered i-ZnO as window layer

for electrodeposited CIGS absorber[12]. While the ED method requires a conducting substrate and

the local fluctuation in conductivity of the substrate (especially after the coating of i-ZnO layer

with very high resistivity) has significant influence on the homogeneity of the TCO layer. With

the efficiency and uniformity improvement of CIGS absorber, there is an increasing demand

from the industry for simpler and cost-effective methods for the manufacturing of transparent

electrodes (TEs). Apart from the basic requirements of good conductivity and high transmittance

(transparency >80%, sheet resistance <100Ω/$\square$), the maximum processing temperature for a non-

vacuum deposited window layer for CIGS solar cells should not exceed 220°C, because higher

temperatures are detrimental to other semiconductor layers within the devices. Several

candidates such as conducting polymer films[13], carbon nanotube (CNT) films[14], graphene films

or their composites[15], and metal wires have been reported as alternative transparent conducting

materials for doped metal oxides[16]. Among them, Ag NWs is a promising option due to its

excellent optical and electrical properties and ease of low temperature deposition. Ag NWs has

been applied as transparent electrodes in flexible organic solar cells and flexible displays by

several groups [17-19]. Yang Yang's group first studied the application of Ag NWs electrode in

hydrazine processed CIS solar cells[16]. In their work, ITO nanoparticles(NPs) was used as a top

layer for Ag NWs to improve the electric conductivity of the Ag NWs/ITO electrode. Currently,

ITO is the most extensively used TCO in industry. However, the scarce availability in nature and high cost of Indium has prompted investigation into alternative materials with comparable properties. Despite the electrical conductivity of AZO is not as high as ITO, AZO has a higher optical transparency as compared with ITO film of similar thickness. CIGS solar cells using AZO and ITO as electrodes exhibited comparable performance[20]. Furthermore, the low cost and abundant materials of AZO make it the most promising alternative of ITO in photovoltaic industry and it is already widely used as a front contact in CIGS solar cells [21].Moon's group replaced the expensive ITO NPs by cheaper AZO and applied the AZO/Ag NWs/AZO composite as electrode in CIGS solar cells and the best device efficiency of 11.3% has been achieved[22,23]. While in Moon's work, CIGS absorber was deposited by vacuum method, which weakened the low cost advantage of the whole device using Ag NWs based top electrode compared with commercial CIGS solar cells. Manjeet et al. developed a low-cost, low-temperature, and fully printing fabrication processes for CIGS solar cells[24]. In their work, the CIGS device were composed of CIGS nanoparticles, CdS nanoparticles and solution deposited ZnO/AgNWs/ZnO window layer. The whole process was proceeded under ambient conditions and annealed at 250°C. Due to the poor electrical properties of CIGS absorber without high temperature selenization, the best solar cell efficiency of fully printed CIGS solar cells was 1.6%.In the reported work of above groups, spin coating was used to obtain the Ag NWs films. Spin coating is a widely used technique for lab scale, but it is not suitable for scale up in industry due to its high material consumption and the restriction to large-area. In addition, when Ag NWs mesh is used as a top electrode, a protecting layer is required to improve its mechanical and electrical properties. However, it is not necessary to use the three-layer AZO/AgNWs/AZO sandwich structure as reported by other group to form a transparent electrode. Herein our work is

centered on the development and implementation of scalable non-vacuum aerosol assisted chemical deposition processes[25] for the deposition of simplified AgNWs/AZO bilayer TEs and its incorporation into electrodeposited CIGS based devices to produce scalable, low cost, unique, and high efficiency fully non-vacuum fabricated CIGS solar cells. Our work has demonstrated that the novel bilayer structure of AgNWs/AZO is sufficient to act as the TE that produced the all non-vacuum processed solar cells with efficiency of 14.05%, which is much higher than the efficiency reported in the previously reported work. Furthermore, such simplified structure would reduce the processing time and cost.

Experimental

Electro-deposition for CIGS absorber

A 3mm soda-lime glass substrate was coated with a highly conductive molybdenum-based back contact and used as the cathode for the electrodeposition process. Cu-In-Ga metallic layers were deposited successively in order to form a metallic stack with standard Cu/(In+Ga) and Ga/(Ga+In) ratios of 0.9 and 0.4 respectively. Once deposited, the Cu-In-Ga metallic stack was processed in an atmospheric pressure for thermal treatment, taking advantage of being at the same time less hazardous and less expensive. The CIGS absorber was subsequently covered with a 40nm-thick CdS buffer layer. Finally, a standard window layer consisting in 80nm i-ZnO and 450nm of AZO was sputter-deposited on top of the buffer to produce a reference cell. The chosen thicknesses of i-ZnO and AZO were optimum for our cell design with the chosen grid spacing given the conductivity & transparency requirements. This may not apply to all CIGS cells as there are many specific aspects to optimize for the front window layer (conductivity, transparency, process time, cost).The i-ZnO helps to ensure that there are no shunts between the

conductive layer and CIGS (especially true for thin emitters such as CdS), thus the optimal thickness must be high enough to improve the shunt resistance while not too high to prevent an increase in series resistance. The AZO layer must be thick enough to sufficiently conduct the electrons to the grid fingers while letting as much light as possible enter the cell. The thicknesses of the i-ZnO and AZO layers must be tuned in order for the optical interferences to give a maximum value (optical transmission) for a wavelength well converted by the cell, usually around 600-700nm.In the case of samples processed with non-vacuum deposited TEs, the standard fabrication process was stopped at NEXCIS after CdS deposition. Then both i-ZnO layer and the transparent conducting layer consisting of Ag NWs based nanocomposite were deposited by non-vacuum aerosol assisted chemical based method.

Preparation of Al-doped ZnO (AZO) and i-ZnO precursor solutions

The Al-doped ZnO and i-ZnO precursor solutions were prepared by simply dissolving zinc acetate dihydrate and aluminum chloride hexahydrate in ethanol/ methoxyethanol based solvent. Ethanolamine was used as complex agent.In preparing AZO precursor solution, the amount of aluminum, defined as [Al]/[Al + Zn], was kept at 1.0 at%. For the preparation of i-ZnO precursor solution, no Al precursor was added.

Deposition of Ag NWs based TEs

Ag NWs solution (length circa. 25 μm, and diameter circa. 90nm from BlueNano) was first dispersed in ethanol based solvent with a concentration within 0.01-0.1mg/ml, and it was subsequently spray-deposited using aerosol assisted chemical deposition setup onto Mo coated glass with CdS covered CIGS substrate. The deposition continued until the desirable conductivity of the film was achieved. After deposition, Ag NWs was annealed at 180℃ for 2-5

mins to improve the sheet conductance. The adherence and conductivity of Ag NWs layer was further improved by depositing a thin layer of AZO film on top of it by aerosol assisted chemical deposition. In order to remove any remaining organic residues in AZO layer, the deposited AZO layer was thermally treated at 200℃ for 3-10 mins followed by UV treatment for 6mins.

In order to improve the device performance, a thin layer of i-ZnO was applied between CdS and TE layer. I-ZnO layer was deposited using the same deposition method for AZO thin films. In order to achieve the desired quality and thickness, i-ZnO was deposited via multi-cycle followed by thermal treatment at 200℃ for 3-10 mins and UV treatment for 6min after each cycle of film deposition. The surface of ZnO is very easy to absorb O_2, which forms charge trap states and results in lower carrier concentration. UV treatment can desorb O_2 and free the electrons from charge trap states on the ZnO surface, thus it passivates the possible electron traps in the film[26]. Further post device thermal treatment at 220℃ for a few mins was also being carried out to increase the connection between the overlapping Ag NWs and to remove any organic residues in i-ZnO layer. 220℃ as chosen because higher temperatures (above 220℃) might lead to elemental diffusion between CIGS/CdS interface and cause the undesirable degradation of solar cell performance.

Structure, optical and electrical characterization

The surface morphology of the as-produced Ag NWs based TE thin films was characterized using scanning electron microscope (SEM, JEOL JSM-6480LV). The surface roughness of Ag NWs based films was characterized using atomic force microscopy (AFM, Veeco CP-Research Scanning Probe Microscope, contact mode). Transmission electron microscopic (TEM) image was obtained by JEOL 2000FX where the sample was prepared using the same fabrication

method on glass substrate but directly depositing the related film on copper grids instead. The optical transmittance spectra was analyzed by a PerkinElmer S750 UV-Vis spectrometer. The conductivity of TEs was measured by four-probe method.

Solar cells of 4.5x4.5mm^2 were manufactured by manual mechanical scribing and the efficiency of solar cells was measured at 100mW/cm^2 under AM1.5 simulated sunlight illumination.

Results and discussion

The sheet resistance of Ag NWs film can be adjusted by the time of spray-deposition. Longer deposition time leads to higher surface coverage ratio and lower sheet resistance of Ag NWs. While the enhanced amount of Ag NWs can also lead to lower transmittance due to the corresponding shadow effect. Ag NWs based TE films with different transmittances and sheet resistances were fabricated in order to obtain the optimum transmittance in the region important for CIGS absorption (i.e.400-1200nm), while keeping resistivity low enough for efficient electron transport and collection. SEM images of TEs with different sheet resistance are shown in Figure.1a-c. The transmittance of Ag NWs based TEs with different sheet resistance is shown in Figure 1d. For all of the Ag NWs based TEs, there is a plasmon absorption at wavelengths $\lambda <$ 450nm (with the maximum resonance around $\lambda = 380$ nm). Compared with ITO or AZO TEs, one advantage of Ag NWs based TEs is that the absorption or transmission spectral is completely flat in the visible regime from 550nm towards near IR. The absorption in this spectral regime originates from the geometrical coverage of the Ag NWs. The spray deposited Ag NWs were loosely connected with each other. The contact resistivity of the Ag NWs junction has notable impact on the conductivity of the whole Ag NWs layer. When a thin layer of AZO was deposited by wet chemical method on top of Ag NWs, the gradual drying of the solvent of AZO solution

provides a capillary forces, which lead to aggregation of AZO around the Ag NWs and thus bind

the Ag NWs together. The tightening of the connection between Ag NWs increased the

conductivity of Ag NWs layer. In addition, the closely connected Ag NWs increased the

transmittance of Ag NWs layer. The comparison of transmittance plotted as a function of the

sheet resistance for Ag NWs film and AgNWs/AZO nanocomposite electrode is shown in Figure

1e. It is demonstrated that the coating of a thin layer of AZO on top of the non-vacuum deposited

Ag NWs thin film not only increased the conductivity of the composite film but also increased a

little of the transmittance of Ag NWs based transparent conducting electrode over 550nm due to

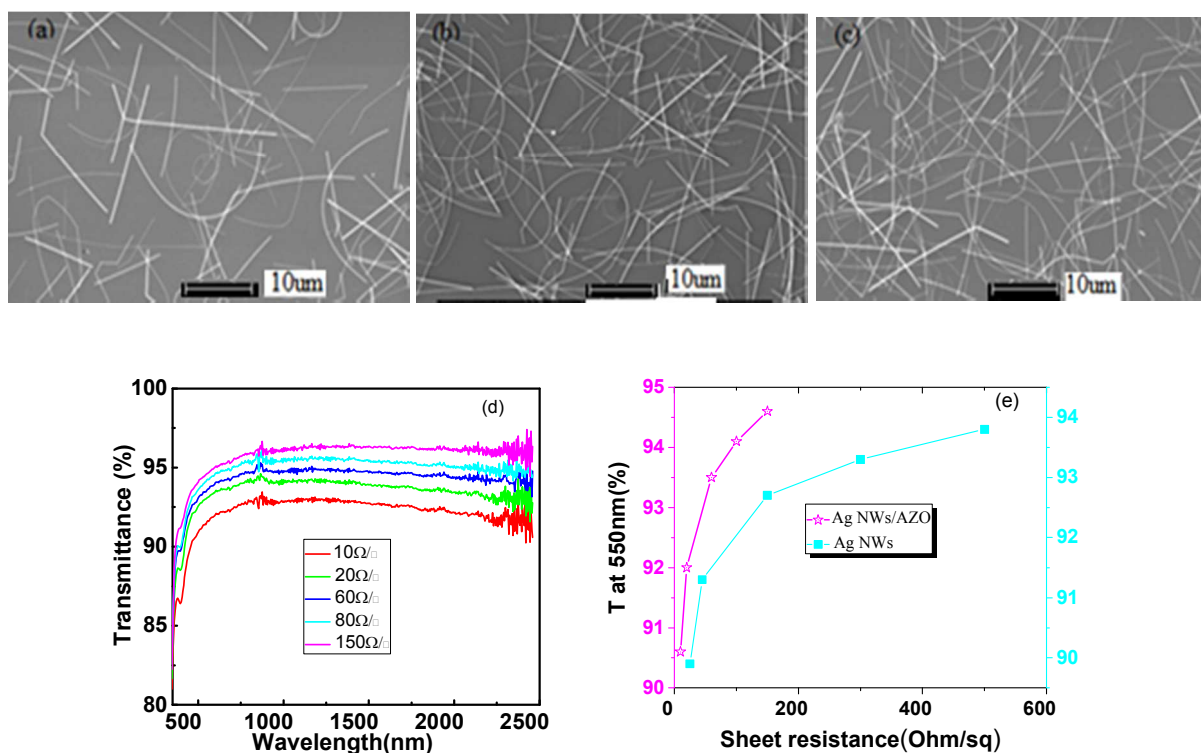tightening of the connection between AgNWs by AZO top layer.

Figure 1. (a)SEM images of morphology of Ag NRs TEs with sheet resistance of (a) 500 Ω/□
(b) 60 Ω/□ (c) 20 Ω/□ .(d)Transmittance of Ag NWs based TEs with different sheet
resistances.(e)Transmittance(T) plotted as a function of the sheet resistance for Ag NWs film and
AgNWs/AZO nanocomposite electrode

Analysis of the surface morphology of Ag NWs based TEs was performed by AFM.AFM images in Figure 2a and Figure 2b show a reduction of the mean surface roughness (Rms) from circa. 70.4nm for untreated Ag NWs based films to circa.27.6nm for AZO coated AgNWs. AZO was found covered on top of the AgNWs, forming a protective layer for Ag NWs mesh. The resulting Ag NWs/AZO nanocomposite films possess an increase in mechanical and thermal stability, with an obvious decrease in surface roughness. In order to better understand the principle of the decrease of sheet resistance and surface roughness for Ag NWs film after coating with a layer of AZO film on top of it, TEM was used to characterize the morphology of prepared Ag NWs /AZO composite thin films and the related image is shown in Figure 2c. Ag NWs /AZO composite sample for TEM was directly deposited on carbon coated Cu grid. Except for the wire shape Ag NWs, it also can be clearly seen from the TEM image that there was a layer of AZO thin film filling the voids between Ag NWs (also shown in FigureS1 and FigureS2). This AZO film at joining points of Ag nanowires can act as glues to fix the positions of Ag NWs and help to bind the crossed Ag NWs together and tighten intimate contact between Ag nanowires, which can increase the lateral conductivity of Ag NWs thin films. Moreover, the thin AZO film formed between the substrate and Ag NWs, can help Ag NWs to stick onto the substrate with improved adhesion and better collection of electrons. In order to confirm that AZO layer is uniformly covered on Ag NWs, EDX mapping image of Ag, O, and Zn elements of Ag/AZO composite on glass substrate was investigated (Figure2 d-g).Figure 2d shows the back scattering electron (BSE) SEM image of an approximate area of 6μmx6μm.The Ag element mapping shown in Figure 2f is consistent with a wire pattern shown in SEM image. While the mapping of O and Zn elements throughout of the area is obviously different from that of the wire pattern of Ag element, and a uniform and continuous distribution of Zn and O element is demonstrated in

Figure 2f and Figure 2g, These results indicated that a continuous and uniform AZO layer was coated on Ag NWs.
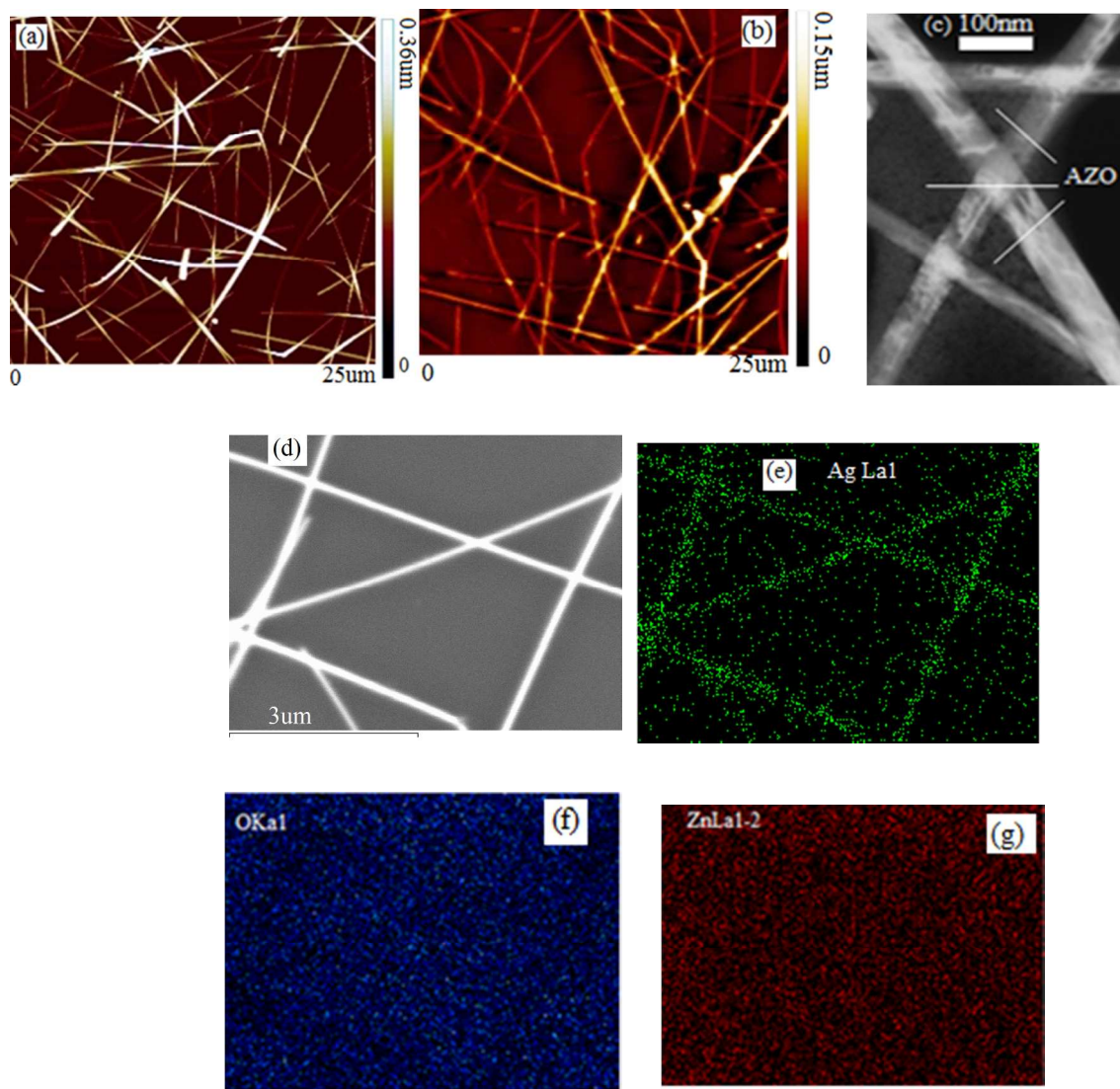

Figure 2. AFM images for (a)AgNWs film and (b)AgNWs/AZO film on glass. (c) TEM of Ag NWs based transparent conducting electrode. (d)SEM(BSE) image and EDX element mapping(e:Zn, f:O, and g:Zn) of Ag NWs based transparent conducting electrode on glass slide

The direct deposition of AgNWs based TEs onto Nexcis's Glass/Mo/CIGS(electrodeposited)/CdS(chemical bath deposition) sample without i-ZnO layer exhibited poor performing photovoltaic devices (ca. 4% conversion efficiency). Therefore, an i-

ZnO layer is required to prevent the leakage current between the buffer layer and top electrode of CIGS solar cells, which can reduce possible carrier recombination and obtain a better band alignment at the CdS interface. In this respect,we explored the development of fully non-vacuum fabricated CIGS solar cells by fabricating i-ZnO using non-vacuum method. The thickness of i-ZnO layer in reported high efficiency devices varied from 50nm to 100nm due to the different thickness of CdS and different film quality of the CIGS absorber layer[27,28,29]. Thicker i-ZnO layer could efficiently avoid the shunt current; while too thick i-ZnO layer leads to lower current resulted by higher optical loss and higher series resistance in the device. Considering the possible existence of organic residue in the non-vacuum processed i-ZnO layer, the thickness of i-ZnO layer was designed to be below 50nm.A series of solar cells with different thicknesses of i-ZnO layer were prepared.   The photovoltaic properties of these all non-vacuum solar cells are presented in Figure 3 and Figure 4. A statistical photovoltaic study has been performed on 9 of pixel cell for each sample. The J-V characteristics were derived from the best performing photovoltaic devices. The CIGS solar cells with i-ZnO layer showed better photovoltaic properties than the cell that without i-ZnO layer. With the increase of the thickness of i-ZnO layer from 0 nm to 45 nm, the open circuit voltage (Voc) of CIGS solar cells increased obviously from 0.41V to 0.59V. The related device efficiency (η) increased from 3.84% to 12.12%, which is the result of combined effect of the improved fill factor (FF), short circuit current (Jsc), and Voc. Further increase of the thickness of i-ZnO layer from 45nm to 60nm leads to a decrease instead of further increase of the solar cell efficiency. This might due to that the thicker i-ZnO layer (60 nm thick) could lead to higher series resistance in the whole device and result in lower Jsc and FF as compared with fully non vacuum processed CIGS solar cell with a thinner i-ZnO layer (45nm thick). Based on the above photovoltaic results, the thickness of i-ZnO in fully non-

vacuum processed CIGS solar cells was not further increased and controlled around 45nm in the
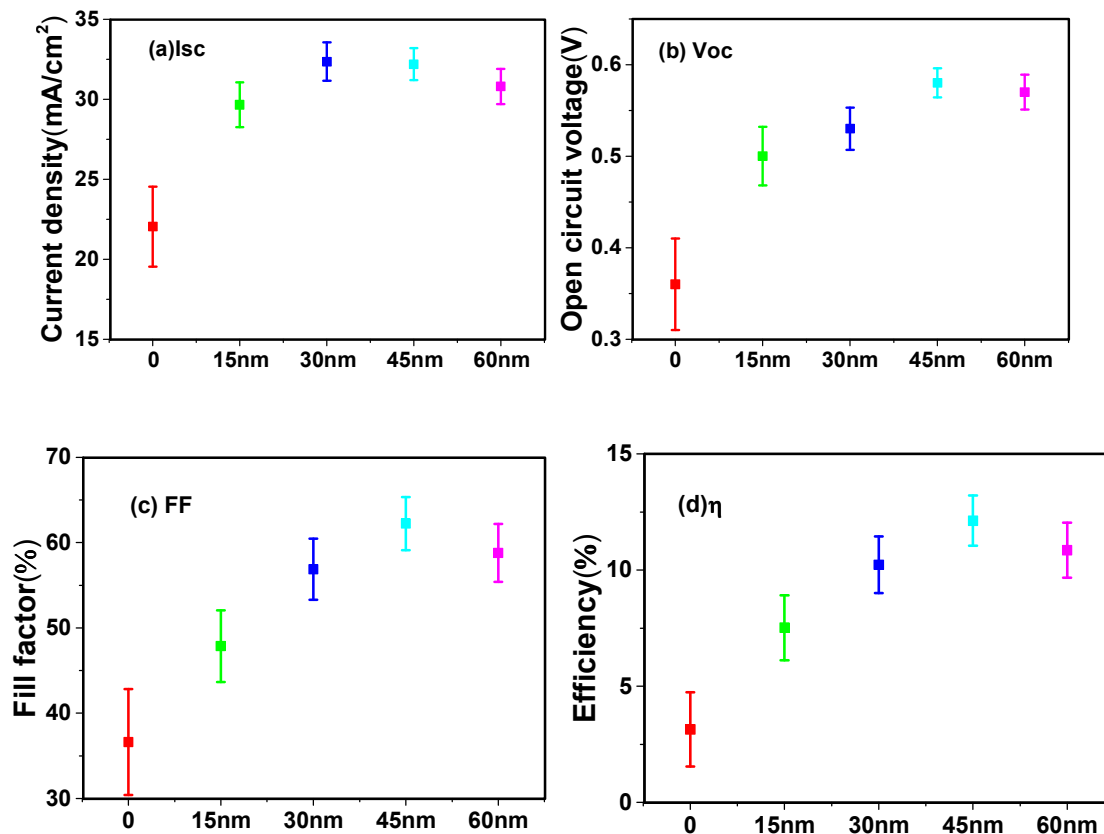
following work.

Figure 3. (a) Jsc, (b)Voc, (c)FF and (d) η of fully non-vacuum fabricated CIGS solar cells

consisting of i-ZnO layers with different thicknesses.

The device structure of the non-vacuum fabricated CIGS (except back-contact) photovoltaic with

a structure of AZO/AgNWs/i-ZnO/CdS/CIGS/Mo/Glass is shown in SEM image in Figure

4b.From the top surface, it can be clearly seen the conducting network formed by Ag NWs .The

Ag NWs are covered by a layer of densely deposited AZO thin film, which would improve the

adhesion between the nanowires and the underneath parts of the device. As it is shown in the top

SEM image, there is a lot of void space between Ag NWs in the transparent electrode. In the case

of transparent electrode without AZO top layer, the photo-produced electrons only can be collected by AgNWs, so the charge collection efficiency is very low. Ag NWs networks with a thin layer of AZO covering the void spaces can ensure effective charge carrier collection in solar cells, due to the fact that the produced electrons can be easily extracted through both AgNWs and the AZO layer between Ag NWs. Grain boundaries of CIGSSe layer may act as recombination centers for photo-generated charge carriers, resulting degradation of device photovoltaic performance. It is desirable to have grain sizes about the order of the film thickness to minimize such recombination effects. Cross-section SEM shown in Figure 4(b) demonstrated that CIGS absorber layer is of good crystalline quality with grain size circa. 1μm, which meets the requirement of grain size for high efficiency CIGS solar cells. Both the i-ZnO and AZO layers are too thin(<50nm) to be separated from Figure 4b. A schematic diagram in Figure 4c illustrates the structure of i-ZnO/AgNWs/AZO window layer, which is composed of a conducting Ag NWs mesh sandwiched between a bottom layer of i-ZnO and a top layer of AZO. The role of i-ZnO layer is to avoid the shunt circuit in the device as in vacuum processed CIGS solar cells. While AZO layer performs multi-function such as to increase the adherence of Ag NWs with the bottom layer, protect the Ag NWs mesh from thermal and mechanical damage, and improve lateral charge collection in solar cell device.

1
2
3
4
5
6
7
8
9
10
11
12
13
14
15
16
17
18
19
20
21
22
23
24
25
26
27
28
29
30
31
32
33
34
35
36
37
38
39
40
41
42
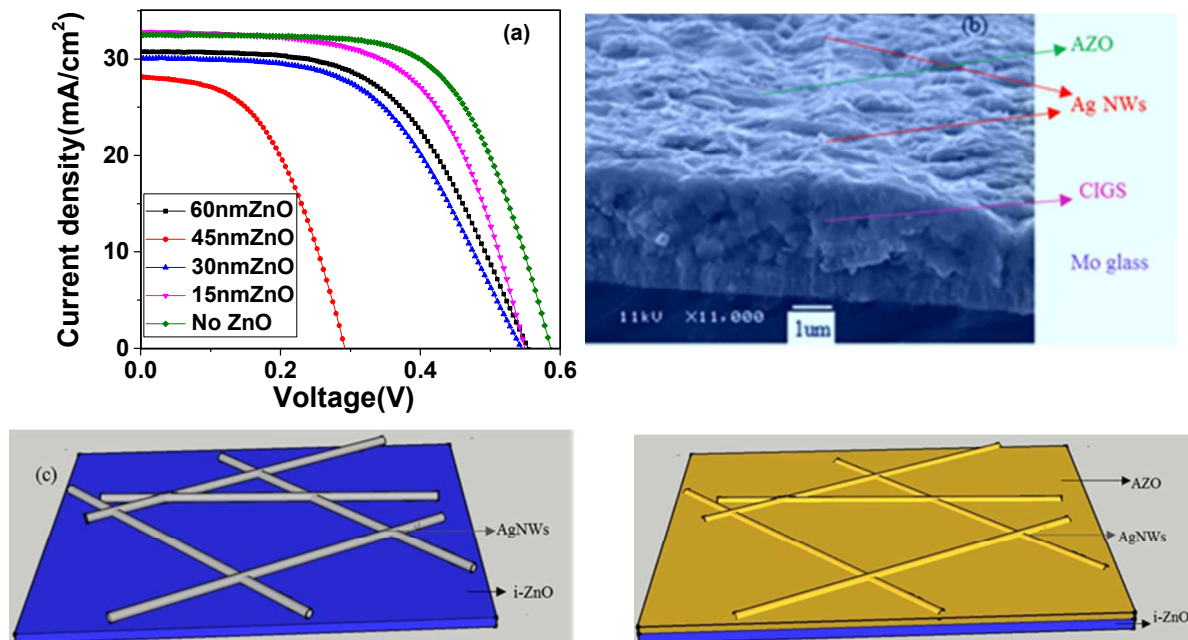43
44
45
46
47
48
49
50
51
52
53
54
55
56
57
58
59
60

Figure 4. (a) J-V characteristics of the fully non-vacuum fabricated CIGS cells containing i-ZnO

layers with different thicknesses. (b) Cross-section SEM of the device structure of fully non-

vacuum CIGS solar cells(c) Scheme of the structure of i-ZnO/AgNWs/AZO window layer

In the all non-vacuum processed CIGS solar cells, the sheet resistance and transmittance of the

Ag NWs/AZO top electrode also have great influence on the device performance. The normal

requirement of the sheet resistance of TCO in CIGS solar cells should be less than 100Ω/□.

AgNWs/AZO TEs with sheet resistance of 10, 20 and 80 Ω/□ was prepared and the influence of

the optical transmittance and sheet resistance of Ag NWs based TEs on solar cell performance is

presented in Figure5 and Table1. TE with lower sheet resistance leads to more efficient current

transport and collection from the buffer layer to the top electrode. When the sheet resistance of

AgNWs based TEs decreased from 80 Ω/□ to 20 Ω/□, the Jsc and FF of the devices increased

from 30.06 mA/cm^2 and 0.59 to 33.66mA/cm^2 and 0.66 respectively. The related efficiency in

the above two devices increased from 10.27% to 13.28% ,which is mainly the resultant of the

decrease of the series resistance (Rs) in the devices from 29.16 $\Omega.cm^2$ to 15.67 $\Omega.cm^2$. Due to the decreased transmittance of TE layer, further decrease of the sheet resistance from 20 $\Omega/\square$ to 10 $\Omega/\square$ decreased the Jsc and efficiency of the devices (as shown in Table1) .From the above results, it can be concluded that the optimized sheet resistance of AgNWs/AZO TE for all non-vacuum CIGS solar cells is 20 $\Omega/\square$, with a transmittance of 92.0% at 550nm. The transmittance at 550 nm wavelength is normally used to demonstrate the transmittance of conducting electrode (especially for CIGS solar cells). Since light of 550nm wavelength is the average wavelength of visible light and is the most sensitive to human's eyes.

Except for the thickness of i-ZnO layer, another factor could influence the device performance of fully solution processed CIGS solar cells is the properties of AZO top layer. For AgNWs/AZO electrode, its sheet resistance is mainly determined by the surface coverage ratio of Ag NWs, and the thickness of AZO has little effect on Rsh of the whole layer. AZO layer as a protecting layer in the composite electrode should be thick enough to form a continuous top layer. While in CIGS solar cells, due to the limited surface coverage ratio of Ag NWs, the photoelectrons generated far from the Ag NWs must move laterally to reach the Ag NW network to be collected (Figure 5b). Koishiyev et al. has studieded the impact of sheet resistance (Rsh) on 2-D modeling of thin-film solar cells[30]. It was reported that for CIGS solar cells, $Rsa \cong \rho_s L^2/2$, where Rsa is the additional series resistance component introduced by the lateral current flow through AZO layer, ρ_s is the sheet resistance of charge transfer from AZO layer to Ag NWs and L is the lateral traveling distance required to reach the nearest AgNWs. From SEM image in Figure 1c, it can be found that the L ranged from 1μm to 10μm in Ag NWs composite films with 20$\Omega/\square$.The series resistance (Rs) of the reference CIGS cell is around 9.58 $\Omega.cm^2$ (from Table 2), so the Rsh of AZO layer should be at least below a few of M$\Omega/\square$ in order to not affect the Rs in the solar cell

device. A few micrometer thickness of AZO deposited by wet chemical method such as spray pyrolysis can reach the sheet resistance below 100 $\Omega/\square$ after thermal treatment[31]. Based on the above theory, tens of nm of good quality AZO should be thick enough for efficient lateral charge collection of Ag NWs/AZO electrode. As mentioned earlier, the process temperature of window layer for CIGS solar cells should not exceed 220°C. The thicker the modified chemical deposited AZO layer, the longer time and higher temperature for the thermal treatment to remove organic residues. Due to the above reasons, the thickness of AZO layer was chosen at 30nm which is thick enough to form a continuous protecting layer for Ag NWs mesh. From the photovoltaic parameters shown in Table1, it can be found that the FF in device using Ag NWs/AZO based electrode(20 $\Omega/\square$) is 65.57, which is not much lower than the FF(71.22) of reference device using sputtered AZO. Considering the existence of organic residues in AZO layer, instead of changing the thickness of AZO layer, after-device thermal treatment was adopted to further remove the organic residues and improve the quality of modified chemical deposited AZO and improve the device performance.
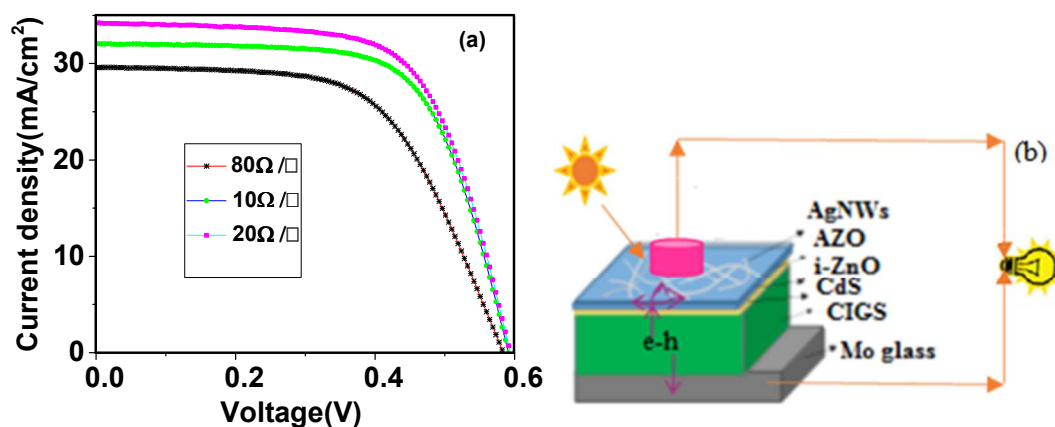
Figure 5. (a)J-V curve of CIGS cells using Ag NWs based TEs with different Rsh(b) Scheme of the device structure and work principle of fully solution processed CIGS solar cells

Table 1 Efficiency (η), Voc, Jsc and FF of CIGS cells using Ag NWs based TEs with different optical transmittance and sheet resistance

Sample	Jsc(mA/cm²)	Voc(V)	FF(%)	η(%)	Rs(Ω.cm²)	Rsh(Ω.cm²)
10 Ω/□	31.71	0.59	66.70	12.63	15.92	7906
20 Ω/□	33.66	0.59	65.57	13.28	15.67	4278
80 Ω/□	30.06	0.58	59.38	10.27	29.16	5216
Reference cell	0.60	33.93	71.22	14.45	9.58	3687

In order to make the developed process for all non-vacuum CIGS solar cells compatible for scale up in the future, after device fabrication, another thermal treatment at a little higher temperature was conducted to improve the uniform efficiency distribution of solar cells on 5cmx5cm substrate. Thermal treatment of devices at 220℃ for couples of minutes was performed in glovebox to remove any organic residues in ZnO layer. 220   was chosen because temperature above 220   might lead to the undesirable elemental diffusion between the CIGS/CdS interface and cause the degradation of solar cell performance. J-V curve of one of the low efficiency device before and after thermal treatment is shown in Figure 6(a) and the corresponding PV parameters are summarized in Table 2. With after-device thermal treatment, there is a little increase of Voc from 0.57V to 0.58V, an obvious increase of Jsc from 28.48 mA/cm² to 32.78mA/cm², and a huge increase of FF from 47.30% to 68.11%, which has led to an increase in device efficiency from 7.68% to 12.95%. Photovoltaic parameters in Table 2 demonstrated that the increase of the device efficiency after-device thermal treatment is mainly because of the very obvious decrease of Rs in the cell, which is responsible for the increase of Jsc and FF due to the effective collection of electrons. The minor increase of Voc might be related with less defect and lower charge recombination centers after the remove of organic residues through thermal treatment. The comparison of the best performance fully non-vacuum fabricated solar cell with

the reference solar cell consisting of electrodeposited CIGS with the sputtered i-ZnO/AZO window layer is also shown in Figure 6(b). The best performance of the fully non-vacuum fabricated CIGS solar cell shows efficiency of 14.05% with Jsc of 34.82mA/cm^2, Voc of 0.58V and FF of 69.60% respectively, which is comparable with the 14.45% efficiency of the reference cell with vacuum processed window layer. Compared with reference cell using sputtered window layer, the fully non-vacuum processed device shows a little higher Jsc due to the better optoelectric properties of Ag NWs electrode. The Voc and FF of the fully non-vacuum processed device can be further increased by optimizing the structure and process of Ag NWs based TEs.

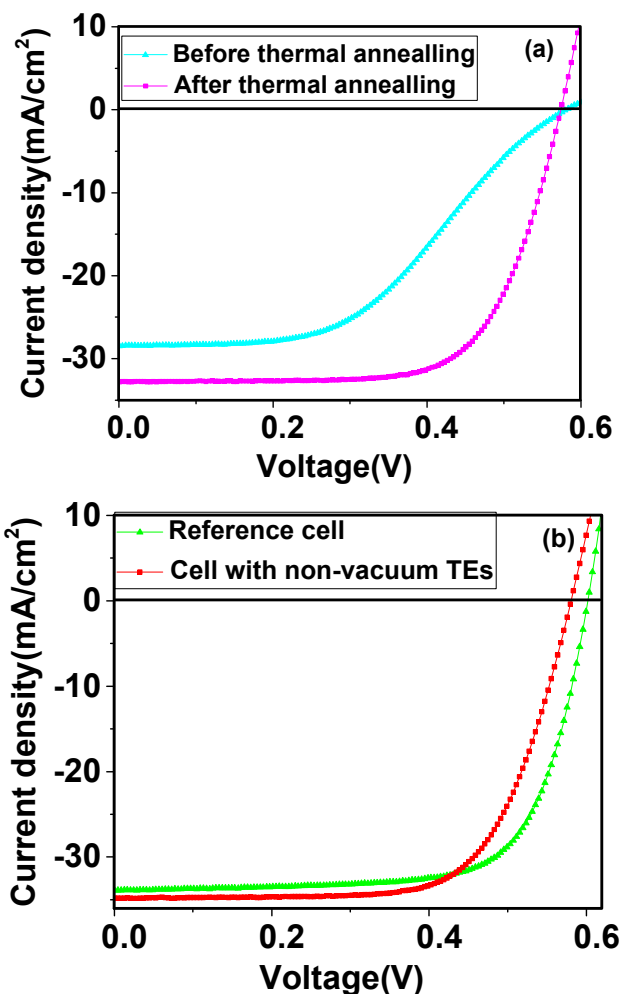**Figure 6.** J-V curve of: (a) Fully non-vacuum CIGS solar cell before and after thermal treatment;

(b) comparison of the best performance fully non-vacuum fabricated solar cell with the reference

CIGS solar cell containing a sputtered i-ZnO/AZO window layer.

Table 2 Photovoltaic parameters of CIGS solar cells in Figure6

Sample	Voc (V)	Jsc (mA/cm²)	FF (%)	Eff (%)	Rs ($\Omega.cm^2$)	Rsh ($\Omega.cm^2$)
Before thermal treatment	0.57	28.48	47.30	7.68	62.21	3122
After thermal treatment	0.58	32.78	68.11	12.95	15.68	7126
Best fully non-vacuum fabricated cell	0.58	34.82	69.60	14.05	12.23	7680
Reference cell using sputtered i-ZnO/AZO	0.60	33.93	71.22	14.45	9.58	3687

The efficiency distribution of fully non-vacuum fabricated CIGS solar cells on 5cm x 5cm

substrate before and after thermal treatment is shown in Figure 7. It can be found that the

efficiency of unit cell increased from 7-12% to 10-13% with after-device thermal treatment. Both

the efficiency uniformity distribution and the absolute value of efficiency were greatly improved

after remove of the organic residues. The performance of the all non-vacuum processed CIGS

solar cells could be further improved by optimizing the thermal treatment of i-ZnO and AZO

layer or selecting good electron transport film which can be processed with good quality below

200℃. For example, laser annealing of i-ZnO and AZO layer could completely remove the

organic residue and increase the crystallization of TEs, which should lead to further improved
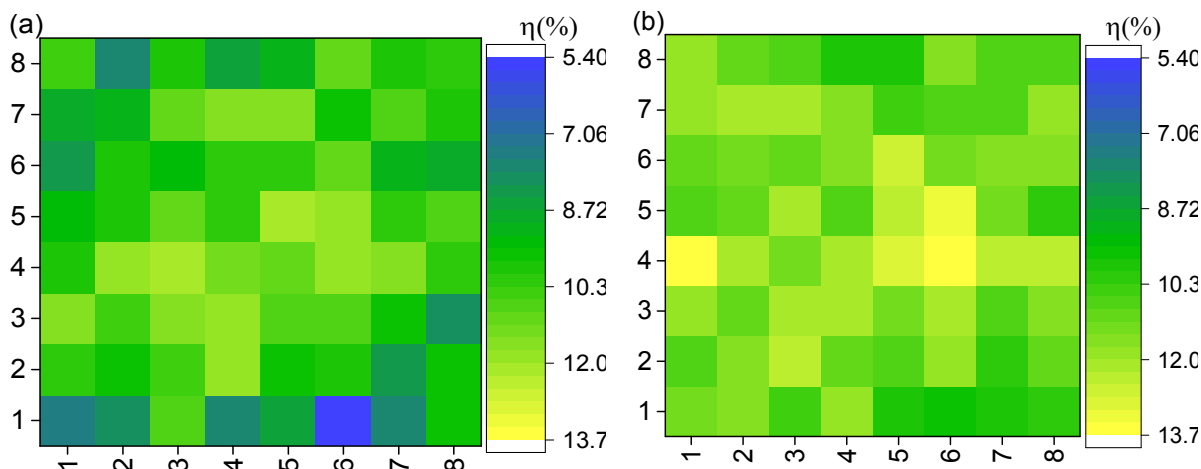
device performance.

Figure 7. Efficiency distribution of fully non-vacuum fabricated CIGS solar cells (on 5x5cm^2 substrate) before (a) and after (b) after device thermal treatment.

Conclusions

In this work, non-vacuum aerosol assisted chemical deposition of novel Ag NWs based transparent conducting electrodes with good transmittance (92.0% at 550nm) and high conductivity (sheet resistance of 20 Ω/□) was developed to replace the sputtered window layer in CIGS solar cells. A thin layer of AZO coating on the Ag NWs network resulted in good connection between the junctions and decreased resistance of the nanocomposite film. Fully non-vacuum fabricated CIGS photovoltaics were fabricated by combining electrodeposited absorber layers with newly developed transparent conducting nanocomposite. A thin layer of non-vacuum deposited i-ZnO with optimized thickness was deposited between CdS and transparent electrode and effectively avoided the shunt current while maintaining high current in the device. After-device fabrication, the subsequent thermal treatment removed the organic residues and improved the performance of CIGS photovoltaic. The best performance of the fully non-vacuum fabricated CIGS solar cells exhibited efficiency of 14.05% with Jsc of 34.82mA/cm^2, Voc of 0.58V and FF of 69.60%, which is comparable with the efficiency of 14.45% of the reference cell with vacuum

sputtered window layer. These promising results open up the possibility of the vision for a fully non-vacuum, environmental friendly and low cost non-vacuum production line of CIGS based solar cells. Experiments are in progress to test the scale up and long-term stability of Ag NWs based transparent conducting electrodes.

ASSOCIATED CONTENT

Electronic Supplementary Information (ESI) available. STEM image (Figure S1) and the related EDX analysis (Figure S2) of the AgNWs/AZO thin film on a carbon coated copper grid. This material is available free of charge via the Internet at http://pubs.acs.org.

AUTHOR INFORMATION

Corresponding Author

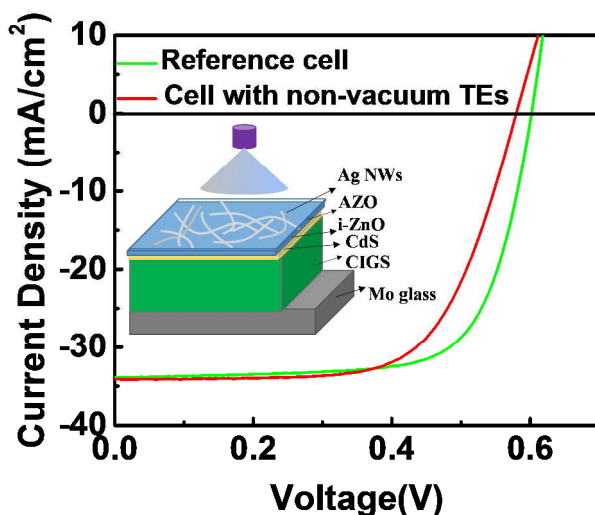*Corresponding author: k.choy@ucl.ac.uk

REFERENCES

(1) Jackson, P.; Hariskos ,D.; Wuerz,R.; Kiowski ,O.; Bauer ,A.; Friedlmeier ,T. M.; Powalla ,M. Properties of Cu(In,Ga)Se$_2$ Solar Cells with New Record Efficiencies up to 21.7% . *Phys. Status Solidi RRL* **2015**,*9*, 28-31.

(2) Bhattacharya, R. N.; Batchelor, W.; Hiltner,J. F.; Sites, J. R. Thin-film CuIn$_{1-x}$Ga$_x$Se$_2$ Photovoltaic Cells from Solution-based Precursor Layers. *Appl. Phys. Lett.* **1999**, *75*,1431-1433.

(3) Barkhouse, D. A. R.; Gunawan, O.; Gokmen, T.; Todorov, T. K.; Mitzi, D. B. Device Characteristics of a 10.1% Hydrazine-processed Cu$_2$ZnSn(Se,S)$_4$ Solar Cell. *Prog. Photovoltaics* **2012**,*20*, 6-11.

(4) McLeod, S. M.; Hages, C. J.; Carter, N. J.; Agrawal, R. Synthesis and Characterization of 15% Efficient CIGSSe Solar Cells from Nanoparticle Inks. *Prog. Photovoltaics* **2015**,*23*,1550-1556.

(5) Uhl, A. R.; Fella, C.; Chirila, A.; Kaelin, M. R.; Karvonen, L.; Weidenkaff, A.; Borca, C. N.; Grolimund, D.; Romanyuk, Y. E.; Tiwari, A. N. Non-vacuum Deposition of Cu(In,Ga)Se$_2$ Absorber Layers from Binder Free, Alcohol Solutions. *Prog. Photovoltaics* **2012**,*20*,526-533.

(6) Brown, G.; Stone, P.; Woodruff, J.; Cardozo, B.;Jackrel, D. Device Characteristics of a 17.1% Efficient Solar Cell Deposited by a Non-Vacuum Printing Method on Flexible Foil .In Photovoltaic Specialists Conference (PVSC), 2012 38th IEEE, June 3−8, 2012; pp 003230−003233

(7) Kapur, V. K.; Bansal, A.; Le, P.; Asensio, O. I. Non-vacuum Processing of CuIn$_{1-x}$Ga$_x$Se$_2$ Solar Cells on Rigid and Flexible Substrates Using Nanoparticle Precursor Inks. *Thin Solid Films* **2003**,*431*,53-57.

(8) Hodes, G.; Engelhard, T.; Cahen, D.; Kazmerski, L. L.; Herrington, C. R. Electroplated CuInS$_2$ and CuInSe$_2$ Layers - Preparation and Physical and Photovoltaic Characterization. *Thin Solid Films* **1985**,*128*,93-106.

(9) Aksu, S.; Pethe, S.; Kleiman-Shwarsctein, A.; Kundu, S.; Pinarbasi, M. Recent Advances in Electroplating Based CIGS Solar Cell Fabrication. *In Photovoltaic Specialists Conference (PVSC), 2012 38th IEEE, June 3−8, 2012; pp 003092−003097.*

(10) Nexcis Photovoltaic Technology Home Page. http://www.nexcis.fr(accessed Oct 23, 2014)

(11) Romanyuk, Y. E.; Hagendorfer, H.; Stucheli, P.; Fuchs, P.; Uhl, A. R.; Sutter-Fella, C. M.; Werner, M.; Haass, S.; Stuckelberger, J.; Broussillou, C.; Grand, P. P.; Bermudez, V.; Tiwari, A. N. All Solution-Processed Chalcogenide Solar Cells - from Single Functional Layers Towards a 13.8% Efficient CIGS Device. *Adv. Funct. Mater.* **2015**,*25*,12-27.

(12) Tsin, F.; Venerosy, A.; Vidal, J.; Collin, S.; Clatot, J.; Lombez, L.; Paire, M.; Borensztajn, S.; Broussillou; Grand, P. P.; Jaime, S.; Lincot, D.; Rousset, J. Electrodeposition of ZnO Window Layer for an All-atmospheric Fabrication Process of Chalcogenide Solar Cell. *Sci. Rep.* **2015**,*5*,8961.

(13) Shin, D.; Kim, T.; Ahn, B. T.; Han, S. M. Solution-Processed Ag Nanowires plus PEDOT:PSS Hybrid Electrode for Cu(ln,Ga)Se$_2$ Thin-Film Solar Cells. *ACS Appl. Mater. Interfaces* **2015**,*7*,13557-13563.

(14)   Contreras, M. A.; Barnes, T.; van de Lagemaat, J.; Rumbles, G.; Coutts, T. J.; Weeks, C.; Glatkowski, P.; Levitsky, I.; Peltola, J.; Britz, D. A. Replacement of Transparent Conductive Oxides by Single-wall Carbon Nanotubes in $Cu(In,Ga)Se_2$ based Solar Cells. *J. Phys. Chem. C* **2007**,*111*, 14045-14048.

(15)   Xu, Q. J.; Song, T.; Cui, W.; Liu, Y. Q.; Xu, W. D.; Lee, S. T.; Sun, B. Q. Solution-Processed Highly Conductive PEDOT:PSS/AgNW/GO Transparent Film for Efficient Organic-Si Hybrid Solar Cells. *ACS Appl. Mater. Interfaces* **2015**,*7*, 3272-3279.

(16)   Chung, C. H.; Song, T. B.; Bob, B.; Zhu, R.; Duan, H. S.; Yang, Y. Silver Nanowire Composite Window Layers for Fully Solution-Deposited Thin-Film Photovoltaic Devices. *Adv. Mater.* **2012**,*24*,5499-5504.

(17)   Song, M.;You, D. S.;Lim, K.;Park, S.;Jung, S.;Kim, C. S.;Kim, D. H.;Kim, D. G.;Kim, J. K.;Park, J.;Kang, Y. C.;Heo, J.;Jin, S. H.;Park, J. H.;Kang, J. W. Highly Efficient and Bendable Organic Solar Cells with Solution-Processed Silver Nanowire Electrodes. *Adv. Funct. Mater.* **2013**, *23*, 4177-4184.

(18)   Kang, S. B.; Noh, Y. J.; Na, S. I.; Kim, H. K. Brush-painted Flexible Organic Solar Cells using Highly Transparent and Flexible Ag Nanowire Network Electrodes. *Sol. Energy Mater. Sol. Cells* **2014**, *122*, 152-157.

(19)   Canlier, A.;Ucak, U. V.;Usta, H.;Cho, C.;Lee, J. Y.;Sen, U.;Citir, M. Development of Highly Transparent Pd-coated Ag Nanowire Electrode for Display and Catalysis Applications *Appl. Surf. Sci.* **2015**, *350*, 79-86;

(20)   Yun,T.Y.; Park,S.R.; Beak,J.Y.; Han,H.J.; Jeon,C.W. Comparison of Aluminum Zinc Oxide and Indium Tin Oxide for Transparent Conductive Oxide layer in $Cu(In,Ga)Se_2$ Solar Cell. *Mol. Cryst. Liq. Cryst.* **2013**, *586*, 82–87.

(21)   Powalla, M.; Witte, W.; Jackson, P.; Paetel, S.; Lotter, E.; Wuerz, R.; Kessler, F.; Tschamber, C.; Hempel, W.; Hariskos, D.; Menner, R.; Bauer, A.; Spiering, S.; Ahlswede, E.; Friedlmeier, T. M.; Blazquez-Sanchez, D.; Klugius, I.; Wischmann, W. CIGS Cells and Modules with High Efficiency on Glass and Flexible Substrates. *IEEE J. Photovolt.* **2014**, *4*, 440-446

(22)   Kim, A.; Won, Y.;Woo, K.;Kim, C. H.;Moon, J. Highly Transparent Low Resistance ZnO/Ag Nanowire/ZnO Composite Electrode for Thin Film Solar Cells. *ACS Nano* **2013**, *7*, 1081-1091

(23)   Kim, A.;Won, Y.;Woo, K.;Jeong, S;Moon, J. All-Solution-Processed Indium-Free Transparent Composite Electrodes based on Ag Nanowire and Metal Oxide for Thin-Film Solar Cells. *Adv. Funct. Mater.* **2014**,*24*, 2462-2471

(24)   Singh, M.;Jiu, J. T.;Sugahara, T.;Suganuma, K. Thin-Film Copper Indium Gallium Selenide Solar Cell Based on Low-Temperature All-Printing Process. *ACS Appl. Mater. Interfaces* **2014**, *6*, 16297-16303.

(25)   Choy, K. L. Chemical Vapour Deposition of Coatings.*Prog. Mater. Sci.* **2003**,*48*,57-170.

(26)   Verbakel, F.; Meskers, S. C. J.; Janssen, R. A. J. Electronic Memory Effects in Diodes of Zinc Oxide Nanoparticles in a Matrix of Polystyrene or Poly(3-hexylthiophene). *J. Appl. Phys.* **2007**,*102*, 083701-1-9

(27)   Repins, I.;Contreras, M. A.;Egaas, B.;DeHart, C.;Scharf, J.;Perkins, C. L.;To, B.;Noufi, R. 19.9% Efficient $ZnO/CdS/CuInGaSe_2$ Solar Cell with 81.2% Fill Factor. *Prog. Photovoltaics* **2008**, *16*, 235-239

(28)   Ramanathan, K.;Contreras, M. A.;Perkins, C. L.;Asher, S.;Hasoon, F. S.;Keane, J.;Young, D.;Romero, M.;Metzger, W.;Noufi, R.;Ward, J.;Duda, A. Properties of 19.2% Efficiency ZnO/CdS/CuInGaSe$_2$ Thin-film Solar Cells. *Prog. Photovoltaics* **2003**, *11*, 225-230

(29)   Jackson, P.; Hariskos, D.;Lotter, E.;Paetel, S.;Wuerz, R.;Menner, R.;Wischmann, W.;Powalla, M. New World Record Efficiency for Cu(In,Ga)Se$_2$ Thin-film Solar Cells beyond 20%. *Prog. Photovoltaics* **2011**, *19*, 894-897.

(30)   Koishiyev, G. T.; Sites, J. R. Impact of Sheet Resistance on 2-D Modeling of Thin-film Solar Cells. *Sol. Energy Mater. Sol. Cells* **2009**,*93,* 350-354.

(31)   Ma, T. Y.; Lee, S. C. Effects of Aluminum Content and Substrate Temperature on the Structural and Electrical Properties of Aluminum-doped ZnO Films Prepared by Ultrasonic Spray Pyrolysis. *J. Mater. Sci.: Mater. Electron.* **2000**,*11*,305-309.

Table of Contents Graphic

1
2
3
4
5
6
7
8
9
10
11
12
13
14
15
16
17
18
19
20
21
22
23
24
25
26
27
28
29
30
31
32
33
34
35
36
37
38
39
40
41
42
43
44
45
46
47
48
49
50
51
52
53
54
55
56
57
58
59
60